Local lattice instability and superconductivity in $La_{1.85}Sr_{0.15}Cu_{1-x}M_xO_4$ (M=Mn, Ni, and Co)

C. J. Zhang and H. Oyanagi*
National Institute of Advanced Industrial Science and Technology, 1-1-1 Umezono, Tsukuba 305-8568, Japan
(Received 5 January 2009; revised manuscript received 13 January 2009; published 20 February 2009)

Local lattice structures of $La_{1.85}Sr_{0.15}Cu_{1-x}M_xO_4$ (M=Mn, Ni, and Co) single crystals are investigated by polarized extended x-ray absorption fine structure. The local lattice instability at low temperature is described by in-plane Cu-O bond splitting. We find that substitution of Mn for Cu causes little perturbation of local lattice instability while Ni and Co substitution strongly suppresses the instability. The suppression of superconductivity by Cu-site substitution is related to the perturbation of lattice instability, indicating that local lattice instability (polaron) plays an important role in superconductivity.

DOI: 10.1103/PhysRevB.79.064521 PACS number(s): 74.62.Dh, 61.05.cj, 64.60.−i, 74.81.−g

I. INTRODUCTION

In recent years there has been a growing interest in the possibility that the metallic phase of cuprate superconductors has an instability toward microscopically phase-separated charge and spin inhomogeneities[1] and that this instability might be related to the high-temperature superconductivity (HTSC) itself.[2] In an inhomogeneity picture, the modulated charges (stripes) could in principle support either superconductivity or charge-density wave.[3] When the stripes are static, charge-density wave overwhelms. However, if the stripes are dynamic, the charge fluctuations might suppress the charge-density wave and open a pseudogap that serves as a precursor for superconductivity. This nanometer-scale phase instability could lead to a strong spin-charge-phonon coupling, giving possible evidence of unconventional electron-phonon coupling in HTSC.

The existence of static stripes is now generally accepted due to the observation of inhomogeneous charge distribution in certain compounds such as $La_{1.6-x}Nd_{0.4}Sr_xCuO_4$ and $La_{1.875}Ba_{0.125}CuO_4$.[4,5] However, dynamic stripes—which are particularly important—are not easily and unambiguously detectable. Due to the absence of a clear experimental signature, the possible existence of dynamic inhomogeneous state has been difficult to establish.[6] So far, dynamic inhomogeneity has been suggested by the observation of a second-order parameter well above T_c. For example, a multicomponent response, as a sign of dynamic inhomogeneous state in $La_{2-x}Sr_xCuO_4$ has been consistently observed in different experiments, such as muon-spin rotation, scanning tunneling spectroscopy, and angle-resolved photoemission spectroscopy.[7–9] In a recent inelastic-scattering study, Reznik *et al.*[10] found a clearly discernible characteristic anomaly in the spectrum of phonons in optimally doped $La_{1.85}Sr_{0.15}CuO_4$. This anomaly indicates the resonance between phonons and the motion of ions that form the copper oxide lattice, reflecting the possible existence of dynamic charge inhomogeneity in optimally doped $La_{1.85}Sr_{0.15}CuO_4$. However, inelastic-scattering measurements do not yield direct information on "modulated" Cu-O bond distances. Clearly, if the charge is inhomogeneously distributed in the CuO_2 plane, such that some copper sites have more charge than others, a modulation of in-plane Cu-O bond length would occur. Thus, a high-precision measurement of the in-plane Cu-O bond-length "distribution" would reveal the possible existence of an inhomogeneous state. In this paper we present an accurate determination of the in-plane Cu-O bond-length modulation by detecting the Cu-O atomic displacements. Splitting of the in-plane Cu-O bond distance below a characteristic temperature T^* is clearly present, providing solid evidence for the existence of local lattice instability in optimally doped $La_{2-x}Sr_xCuO_4$. We also report specific perturbations of local lattice instability by doping with different impurities (Mn, Ni, and Co), which is related to the different behaviors on the suppression of superconductivity. The results strongly suggest that the local lattice instability plays an important role in HTSC.

II. EXPERIMENT

Single-crystal samples of $La_{1.85}Sr_{0.15}Cu_{1-x}M_xO_4$ (M=Mn,Ni,Co) were grown by the traveling solvent floating zone method.[11] For the feed rod, stoichiometric polycrystalline powders of $La_{1.85}Sr_{0.15}Cu_{1-x}M_xO_4$ (M=Mn,Ni,Co) were preheated twice at 1150 °C. X-ray diffraction measurements were performed on these polycrystalline powders in order to confirm that the samples were single phase. Then, an appropriate amount of extra CuO was added into the polycrystalline powder in order to compensate for the loss of Cu during the crystal growth and the mixture was thoroughly ground. The obtained fine powders of each sample were placed into a thin-walled rubber tube and formed into a cylindrical seed rod under hydrostatic pressure. The seed rods were sintered at 1250 °C for 24 h in air. The solvent material with the composition of $La:Sr:Cu:M=1.85:0.15:(4-x):x$ for each x was prepared. We used 0.3 g of the solvent and a $La_{1.85}Sr_{0.15}CuO_4$ single crystal as a seed rod. The single-crystal growth rate of Mn-doped samples was kept constant at 0.2 mm/h, and the growth rate of Ni-doped and Co-doped samples was 0.5 mm/h. In order to eliminate oxygen deficiencies, all the crystals were annealed under oxygen gas flow at 900 °C for 50 h, cooled to 500 °C at a rate of 10 °C/h, and annealed at 500 °C for 50 h. The superconducting transition temperature of the samples was determined by a superconducting quantum interference device (SQUID) magnetometer (Quantum Design, MPMS). The applied magnetic field is 10 Oe with field cooling. The magnetic field is applied perpendicular to the CuO_2 plane.

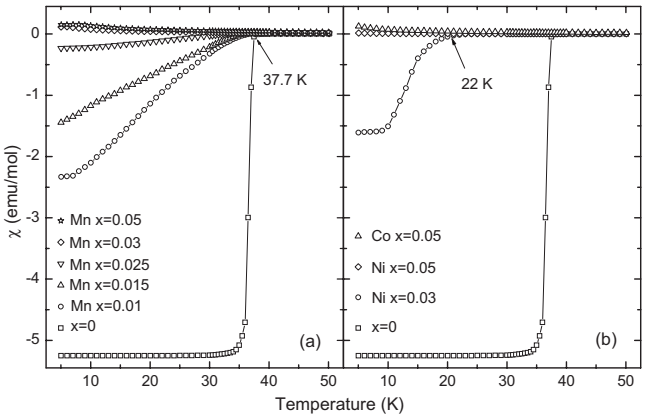

FIG. 1. Temperature dependence of magnetic susceptibility for $La_{1.85}Sr_{0.15}Cu_{1-x}M_xO_4$ (M=Mn,Ni,Co) single-crystal samples. The applied magnetic field is 10 Oe with field cooling. The magnetic field is applied perpendicular to the CuO_2 plane.

Extended x-ray absorption fine-structure (EXAFS) measurements were performed at BL13B at Photon Factory, Tsukuba. The energy and maximum electron current were 2.5 GeV and 400–500 mA, respectively. A directly water-cooled silicon (111) double-crystal monochromator was used, covering the energy range of 4–25 keV. The energy of the incident x-ray was calibrated by assigning the first shoulder of the Cu foil spectrum (Cu K edge) to 8.9803 keV. The energy resolution was better than 2 at 9 keV. The drift in the energy calibration was below 5% of the energy resolution. The number of the counted photons is $\sim 10^8$ photons/s. The sample was mounted in a closed-cycle He refrigerator and the temperature was monitored with an accuracy of ± 0.1 K. The sample sizes were approximately $3\times3\times0.8$ mm^3. The measurements of the in-plane polarized EXAFS spectroscopies were made using polarization of the light parallel to the CuO_2 plane. For the measurements of the out-of-plane polarized spectroscopies, we used a different sample holder so that the electric field of the polarized light is parallel to the c axis of the sample. The details of the experimental setup and data-acquisition process have been described elsewhere.[12] Here we used a state-of-the-art germanium 100-pixel array detector (PAD) collecting signals over a segmented solid angle using a grazing-incidence geometry.

III. RESULTS AND DISCUSSION

A. Local lattice instability in $La_{1.85}Sr_{0.15}CuO_4$

Figure 1 gives the temperature dependence of magnetic susceptibility for $La_{1.85}Sr_{0.15}Cu_{1-x}M_xO_4$ (M=Mn,Ni,Co) samples (Meissner signals). The onset superconducting transition temperature ($T_c^{\rm onset}$) for $La_{1.85}Sr_{0.15}CuO_4$ is 37.7 K. Superconducting transition is observed in $x\leq0.025$ samples of $La_{1.85}Sr_{0.15}Cu_{1-x}Mn_xO_4$. Strikingly, $T_c^{\rm onset}$ remains constant at about 36.5 K in Mn-doped samples, while it decreases rapidly in Ni- and Co-doped samples. For example, the $T_c^{\rm onset}$ value of $La_{1.85}Sr_{0.15}Cu_{1-x}Ni_xO_4$ with x=0.03 is about 22 K. In both Mn- and Ni-doped samples, the superconducting volume fraction decreases with increasing doping content.

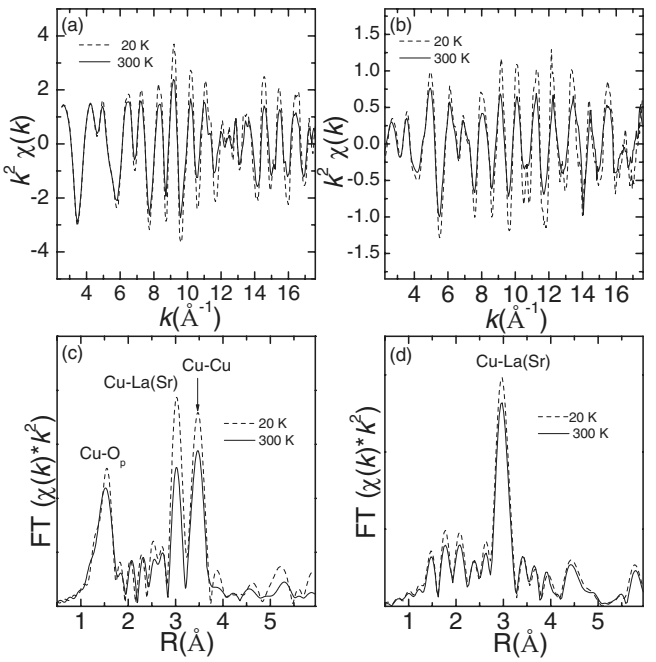

FIG. 2. (a) In-plane polarized Cu K-edge EXAFS oscillations (weighted by k^2) for $La_{1.85}Sr_{0.15}CuO_4$ at 20 K and 300 K. (b) Out-of-plane polarized Cu K-edge EXAFS oscillations (weighted by k^2) for $La_{1.85}Sr_{0.15}CuO_4$. (c) Magnitude of the complex FT of $k^2\chi(k)$ for $La_{1.85}Sr_{0.15}CuO_4$ in the CuO_2 plane at 20 and 300 K. (d) Magnitude of the complex FT along the c axis.

Figures 2(a) and 2(b) show representative examples of the in-plane and out-of-plane polarized Cu K edge EXAFS oscillations (weighted by k^2) of $La_{1.85}Sr_{0.15}CuO_4$, respectively. In both polarization geometries, the EXAFS oscillations taken at 300 and 20 K are shown. The magnitude of the EXAFS oscillations is enhanced at low temperature. Figures 2(c) and 2(d) show the complex Fourier transform (FT) magnitude function of the EXAFS oscillations for $La_{1.85}Sr_{0.15}CuO_4$ with the in-plane and out-of-plane configurations, respectively. The complex FT magnitude function is related to the atomic radial distribution function around the central Cu atom. Compared to the real crystallographic distances, the coordination shell peaks in Figs. 2(c) and 2(d) are shifted to lower R due to scattering phase shifts. In the in-plane configuration, prominent peaks at radii $R\sim1.5$ Å, $R\sim3.0$ Å, and $R\sim3.5$ Å are the Cu-O, Cu-La, and Cu-Cu correlations. In the out-of-plane configuration, the peaks corresponding to the in-plane Cu-O and Cu-Cu correlations are significantly damped. The prominent peak at radius $R\sim3.0$ Å corresponds to the Cu-La correlation. There are several peaks in the $1.3<R<2.2$ Å range where the out-of-plane Cu-O peak appears.

The experimental EXAFS, $\chi(k)$, is analyzed by using of the IFEFFIT analysis package.[13] The fitting of EXAFS data is performed for each orientation by constraining the structural parameters of those paths that contribute to individual polarization. In the in-plane polarization, we fit the experimental data in the $1.0<R<2.0$ Å range. Except the radial distance R and the mean-square relative displacement (MSRD) σ^2, all other parameters are kept constant in the

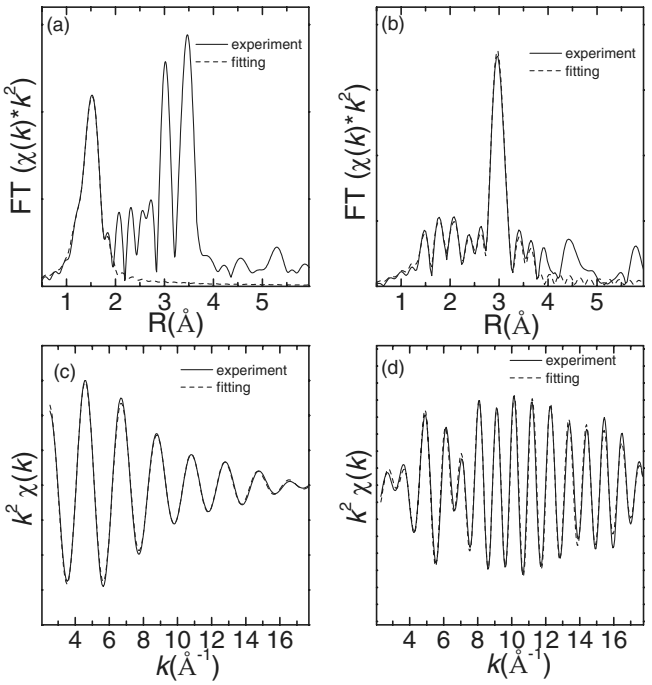

FIG. 3. (a) Comparison of the fitted curve on the nearest-neighbor Cu-O bond (dashed curve) with the experimental FT magnitude function within the CuO_2 plane at 300 K (solid curve). (b) Comparison of the fitted curve with the experimental FT magnitude function along the c axis at 300 K. (c) The back-transformed EXAFS oscillation for the in-plane Cu-O bond at 300 K (solid curve, back transformed over $0.9<R<2.0$ Å). The dashed curve is the fitting result on the Cu-O bond. (d) The back-transformed out-of-plane EXAFS oscillation at 300 K (solid curve, back-transformed over $1.2<R<3.8$ Å). The dashed curve is the fitted curve.

conventional least-squares paradigm. The dashed line in Fig. 3(a) represents a typical curve fitted to the experimental result at 300 K. It can be seen that this curve shows a good agreement with the experimental curve (solid line) in the $1.0<R<2.0$ Å range. For the out-of-plane geometry, we fit the experimental data in the $1.2<R<3.8$ Å range, taking into account the contribution from all possible scattering paths. A typical fitted curve is given as the dashed line in Fig. 3(b). In Figs. 3(c) and 3(d) we compare the fitted curves and

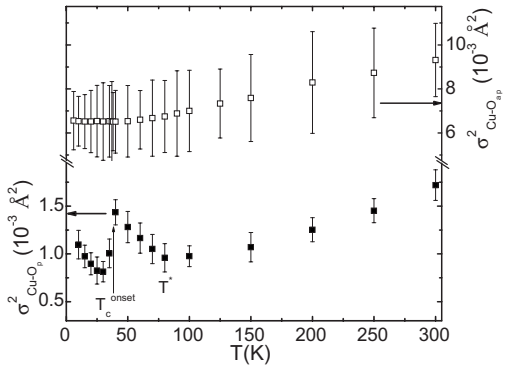

FIG. 4. Temperature dependence of $\sigma^2_{\text{Cu-O}_p}$ and $\sigma^2_{\text{Cu-O}_{ap}}$ for $La_{1.85}Sr_{0.15}CuO_4$. The error bars are estimated from the square root of the diagonal elements of the correlation matrix.

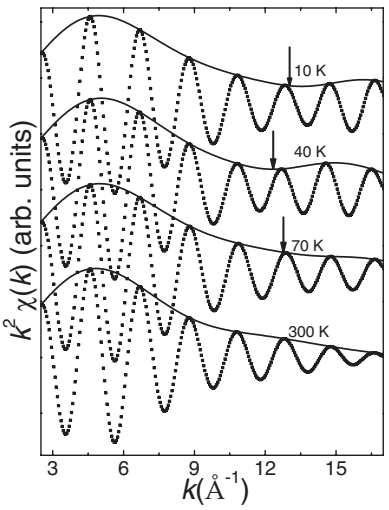

FIG. 5. Fourier-filtered (back-transformed over $0.9<R<2.0$ Å) EXAFS oscillations (scattered dots) and amplitudes (lines) of the in-plane Cu-O_p bond. The changes with temperature in the FT moduli are reflected in the beat at about $k\sim12.5$ Å^{-1}.

experimental data in k space for the in-plane configuration and the out-of-plane configuration, respectively. In both configurations, the fitting curves reproduce the experimental data well.

Figure 4 shows the temperature dependence of MSRD of the in-plane Cu-O bond, $\sigma^2_{\text{Cu-O}_p}$ and the out-of-plane Cu-O bond, $\sigma^2_{\text{Cu-O}_{ap}}$ for $La_{1.85}Sr_{0.15}CuO_4$. In the high-temperature region, $\sigma^2_{\text{Cu-O}_p}$ decreases with decreasing temperature. In contrast, below a characteristic temperature T^* ($T^*\sim80$ K), it exhibits a remarkable upturn, indicating the occurrence of local lattice distortion.[14–17] Previously, a similar local lattice distortion was found and explained by using a two-component model where a distorted local low-temperature tetragonal (LTT) lattice coexists with the undistorted local low-temperature orthorhombic (LTO) lattice.[14] In this study, we systematically analyzed the polarized Cu K-edge EXAFS data along the c axis. In Fig. 4 we also plot the temperature dependence of MSRD of the out-of-plane Cu-O bond $\sigma^2_{\text{Cu-O}_{ap}}$ for $La_{1.85}Sr_{0.15}CuO_4$. We do not observe any anomaly in the temperature dependence of MSRD of the out-of-plane Cu-O bond. This result suggests that the out-of-plane Cu-O bond is not involved in the local lattice instability, i.e., the local lattice distortion occurs within the CuO_2 plane.

Closer examination of the EXAFS oscillations reveals the detailed temperature dependence of the in-plane Cu-O bond distortion. Figure 5 plots the Fourier-filtered (back-transforming over $0.9<R<2.0$ Å) EXAFS oscillations and amplitudes of the in-plane Cu-O bond from 300 to 10 K. It is found that the oscillations are very similar up to $k\sim12$ Å^{-1} at all temperatures. However, for $T<80$ K the local minimum in the amplitude and the irregularity in the phase near 12.5 Å^{-1} constitute a "beat," which signifies the presence of at least two Cu-O shells having different bond distances. Using the relation $\Delta R=\pi/2k$ between the separation of the two shells (ΔR) and the position of the beat (k), the Cu-O distances are determined to differ by ~0.12 Å. Taking into account the average Cu-O bond distance of

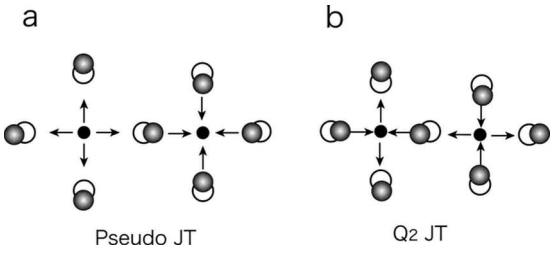

FIG. 6. Schematics of the possible lattice modes describing the oxygen displacements: (a) pseudo-Jahn-Teller mode; (b) Q_2-type Jahn-Teller mode.

$\sim$1.88 Å, the long and short Cu-O bond distances are determined to be $\sim$1.94 and 1.82 Å, respectively. That means, some oxygens are shifted toward or away from their adjacent Cu sites by $\sim$0.06 Å.

The local lattice instability below $T^* \sim 80$ K is described by the in-plane Cu-O bond splitting. Due to the well-known fact that there is no static lattice/charge modulation in optimally doped $La_{1.85}Sr_{0.15}CuO_4$ and the failure to detect the inhomogeneous state by any slow techniques, we suggest that the local lattice instability occurs "dynamically." The dynamic lattice fluctuation time is below the picosecond (10^{-12} s) range, which can be detected only by certain "fast" probes, such as EXAFS and neutron diffraction.[6,18] The powerful fast probes which *freeze* the motion of ions on short timescales ($\sim 10^{-15}$ s), e.g., EXAFS, are eminently suitable for detection of these fluctuation patterns.[18] Lattice instability at this length scale is expected to produce exotic lattice-dynamical properties such as a certain kind of phonon mode softening and strong coupling between the lattice and charge degrees of freedom, leading to polaron formation. Regarding the specific nature of the polaron, two different types of Cu-O bond-stretching modes can be considered as possible candidates: the pseudo-Jahn-Teller mode;[19,20] and the Q_2-type mode.[21,22] These modes are schematized in Fig. 6. Below T_c, the beat feature is weakened but it is still clearly discernible, which indicates the persistence of dynamic lattice instability below T_c. Incidentally the sharp decrease in the local Cu-O lattice displacements was found in ion channeling experiments, where a drop of the variable amplitude at T_c^{onset} was detected.[23] These results indicate that the vibration of planar oxygen becomes silent as the superconducting transition occurs. We conclude that the decrease in vibration is due to the transition of the CuO_2 planar lattice dynamics from an incoherent state to a coherent state as the pairing occurs.

B. Perturbations of local lattice instability by Mn, Ni, and Co doping

Besides the characterization of the in-plane Cu-O bond local lattice instability in $La_{1.85}Sr_{0.15}CuO_4$, another important topic is whether or not and how this local lattice instability relates to the nature of the superconductivity in this system. In the following we investigate some specific perturbations of the local lattice instability by impurity doping. We have used three different transition-metal elements (Mn, Ni, and Co) to replace the Cu in the $La_{1.85}Sr_{0.15}CuO_4$ parent compound. For all the doped $La_{1.85}Sr_{0.15}Cu_{1-x}M_xO_4$ (M=Mn,Ni,Co) single-crystal samples, polarized Cu K-edge EXAFS experiments have been performed from 300 to 5 K, and the same data analysis procedure has been performed. To simplify the data, we plot the temperature dependence of $\sigma^2_{\text{Cu-O}_p}$ for $La_{1.85}Sr_{0.15}Cu_{1-x}M_xO_4$ (M=Mn,Ni,Co) samples in Figs. 7(a) and 7(b). It is found that the doping of Mn, Ni, and Co leads to different perturbations of the local lattice instability. That is, the introduction of Ni and Co dopants at the Cu site strongly depresses the upturn of $\sigma^2_{\text{Cu-O}_p}$ below T^*. With 5% of Ni or Co doping the upturn behavior is completely disappeared. In contrast, the Mn dopant has less perturbation on the upturn behavior. We notice that the upturn of $\sigma^2_{\text{Cu-O}_p}$ is still significant in the 5% Mn-doped sample. In order to see the difference in the perturbation clearly, we fit the temperature dependence of $\sigma^2_{\text{Cu-O}_p}$ for $La_{1.85}Sr_{0.15}CuO_4$ by using the correlated Einstein model,[24] via the following equation:

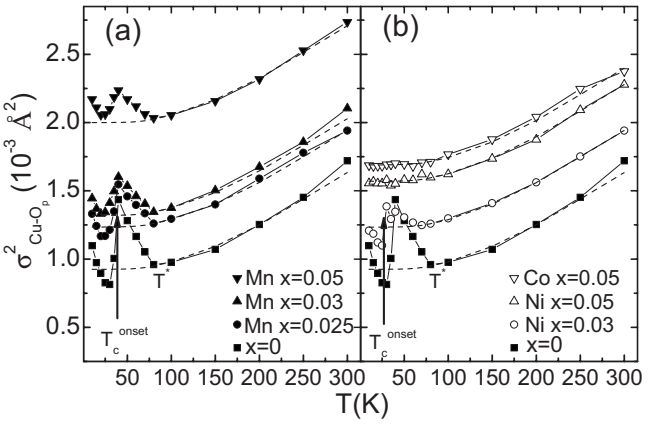

FIG. 7. Temperature dependence of the in-plane Cu-O bond MSRD $\sigma^2_{\text{Cu-O}_p}$ for $La_{1.85}Sr_{0.15}Cu_{1-x}M_xO_4$ (M=Mn,Ni,Co) samples. The dashed lines are the values calculated using Eqs. (1) and (2).

$$\sigma^2_{\text{th}}(T) = \frac{\hbar^2}{2\mu k_B \Theta_E} \coth\left(\frac{\Theta_E}{2T}\right), \tag{1}$$

where Θ_E is the Einstein temperature and μ is the reduced mass of the pair of atoms involved in the bond. The calculated $\sigma^2_{\text{th}}(T)$ curve is shown as the dashed line in Fig. 7. One can clearly see a large deviation between the measured and calculated $\sigma^2_{\text{Cu-O}_p}$ below 80 K due to the occurrence of local lattice instability.

We find that all the dopants (Mn, Ni, and Co) lead to an increase in $\sigma^2_{\text{Cu-O}_p}$, which is likely due to local lattice rearrangement around the dopants. In this case, the $\sigma^2_{\text{Cu-O}_p}$ could be given as a superposition of a temperature-independent term (σ^2_{imp}) and a temperature-dependent dynamic term. For these samples, we also fit the experimental $\sigma^2_{\text{Cu-O}_p}(T)$ curves using a simple equation,

$$\sigma^2_{\text{Cu-O}_p}(T) = \sigma^2_{\text{th}}(T) + \sigma^2_{\text{imp}}. \tag{2}$$

The fitting results are shown as the dashed curves in Fig. 7.

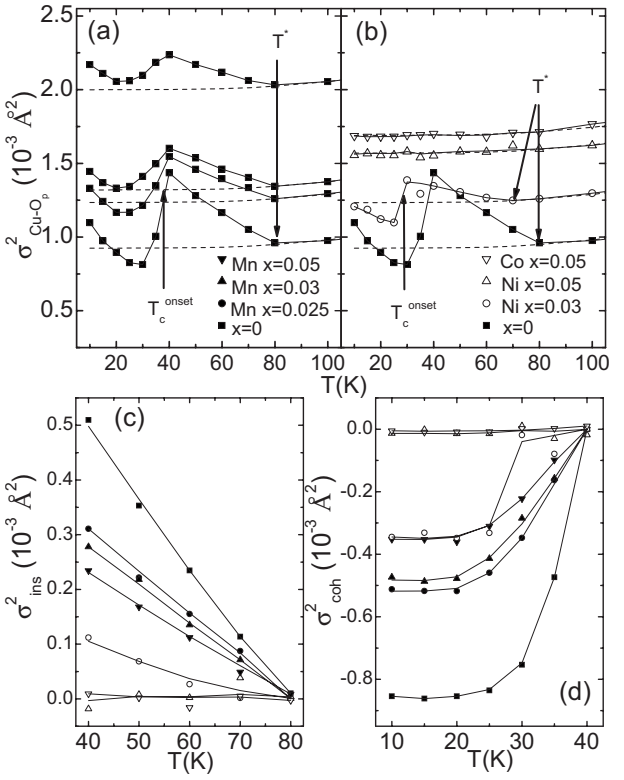

FIG. 8. (a) and (b) Expanded view of the MSRD of the in-plane Cu-O bond, $\sigma^2_{\text{Cu-O}_p}$ for $La_{1.85}Sr_{0.15}Cu_{1-x}M_xO_4$ (M=Mn,Ni,Co) samples below 100 K. (c) and (d) The magnitudes of the upturn at T^* (σ^2_{ins}) and the drop at T_c(σ^2_{coh}) as a function of temperature. The symbols in (c) and (d) are consistent with those in (a) and (b). The dashed lines in (a) and (b) are the calculated values using Eqs. (1) and (2). The solid lines are guides to the eyes.

The detailed variation in $\sigma^2_{\text{Cu-O}_p}$ can be seen more clearly in Figs. 8(a) and 8(b) where the $\sigma^2_{\text{Cu-O}_p}$ values below 100 K are shown. In all Mn-doped samples, the upturn of $\sigma^2_{\text{Cu-O}_p}$ occurs below $T^* \sim 80$ K. In Ni-doped samples, the T^* slightly decreases. For example, the T^* value is about 70 K in 3% Ni-doped sample. It is interesting to notice that the drop of $\sigma^2_{\text{Cu-O}_p}$ occurs at T_c^{onset}. Thus it is clear that the upturn of $\sigma^2_{\text{Cu-O}_p}$ below T^* is due to the occurrence of local lattice instability while the drop of $\sigma^2_{\text{Cu-O}_p}$ below T_c^{onset} is due to the superconducting phase coherence. Using two simple equations we can roughly estimate the magnitudes of the upturn part and the drop part,

$$\text{For } T_c < T < T^*: \quad \sigma^2_{\text{Cu-O}_p}(T) = \sigma^2_{\text{th}}(T) + \sigma^2_{\text{imp}} + \sigma^2_{\text{ins}}(T), \tag{3}$$

$$\text{For } T < T_c: \quad \sigma^2_{\text{Cu-O}_p}(T) = \sigma^2_{\text{th}}(T) + \sigma^2_{\text{imp}} + \sigma^2_{\text{ins}}(T) - \sigma^2_{\text{coh}}(T), \tag{4}$$

where σ^2_{ins} represents the contribution of local lattice instability to the total $\sigma^2_{\text{Cu-O}_p}$, and σ^2_{coh} is due to the phase coherence below T_c. Using Eqs. (3) and (4), we can estimate the magnitudes of σ^2_{ins} and σ^2_{coh} for each sample by subtracting the theoretically modeled Debye-Waller factor from the experimental data. The results are shown in Fig. 8(c) and 8(d).

From Fig. 8(c) one can see that σ^2_{ins} has the largest magnitude in the optimum superconductor $La_{1.85}Sr_{0.15}CuO_4$. With increasing Mn doping, the magnitude of σ^2_{ins} slightly decreases but the contribution from σ^2_{ins} persists in all samples up to x=0.05, indicating that Mn doping does not suppress the local lattice instability. On the other hand, the contribution of σ^2_{ins} decreases rapidly in the Ni- and Co-doped samples. With 5% of Ni(Co) doping the upturn of $\sigma^2_{\text{Cu-O}_p}$ is completely smeared out, indicating that the local lattice instabilities are strongly suppressed by Ni and Co dopants. Figure 8(d) plots the magnitude of the drop of $\sigma^2_{\text{Cu-O}_p}$ due to the superconducting phase coherence below T_c^{onset}. The drop in $\sigma^2_{\text{Cu-O}_p}$ has the largest magnitude in the optimally doped $La_{1.85}Sr_{0.15}CuO_4$ sample. In Ni- and Co-doped samples the magnitude of this drop decreases with increasing doping concentration and finally the drop disappears in nonsuperconducting samples. It is interesting to notice that in Mn-doped samples, the drop in $\sigma^2_{\text{Cu-O}_p}$ is observed in all samples despite the decrease in magnitude.

On the basis of these results we can draw the conclusion that the Mn-doped samples favor the local lattice instability while the Ni and Co dopants are strongly harmful to the local lattice instability. The perturbation of local lattice instability is related to the suppression of superconductivity induced by impurity doping. That is, the introduction of Ni and Co dopants strongly suppresses the local lattice instability and thus severely suppresses the superconducting transition. In contrast to the Ni and Co dopants, the Mn dopants cause less perturbation on the local lattice instability, resulting in a constant onset superconducting transition temperature. It is reasonable to imagine that in Mn-doped samples, the introduction of Mn dopants leads to the separation of the superconducting domains. Near the Mn dopants, regions of nonsuperconducting domains are formed. With increasing Mn doping, more and more nonsuperconducting regions are formed and large superconducting domains could be divided into small superconducting droplets. As the distance between the superconducting droplets becomes large, the tunneling is prohibited and the superconductivity disappears.

C. Local lattice structure around Mn, Ni, and Co dopants

We also investigate the local lattice structures around the Mn, Ni, and Co dopants by analyzing the Mn, Ni, and Co K-edges EXAFS data. Figure 9(a) shows examples of the in-plane EXAFS oscillations (weighted by k^2) for $La_{1.85}Sr_{0.15}Cu_{1-x}M_xO_4$ with x=0.05 at 40 K at the Mn, Ni, and Co K edges. Figure 9(b) gives the Fourier-filtered EXAFS oscillations and amplitudes of the in-plane M-O, (M=Mn,Ni,Co) bond at 40 K. A distinct difference can be seen between the Fourier-filtered EXAFS oscillations of the Ni(or Co)-O bond and that of the Mn-O bond. That is, a "beat" feature is clearly present at $k \sim 10$ Å for the Mn-O bond oscillation, which signifies the presence of two in-plane Mn-O bonds with different distances. The two Mn-O distances are estimated to differ by ~0.16 Å. The beat feature is indiscernible for the Ni(or Co)-O bond case. The tempera-

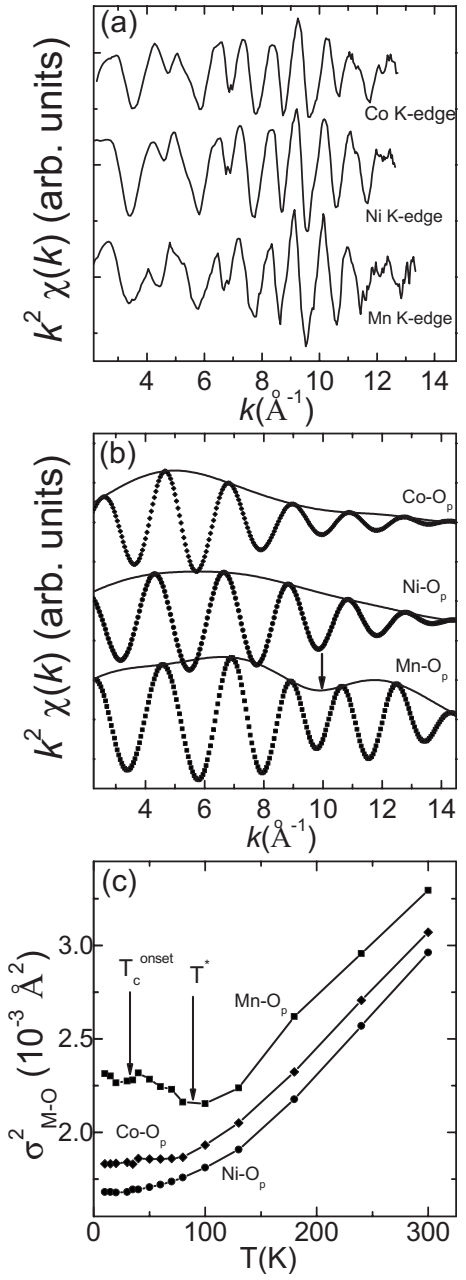

FIG. 9. (a) The in-plane Mn, Ni, and Co K-edges EXAFS oscillations (weighted by k^2) of $La_{1.85}Sr_{0.15}Cu_{1-x}M_xO_4$ (M=Mn,Ni,Co) with x=0.05 at 40 K. (b) Fourier-filtered EXAFS oscillations and amplitudes of the in-plane M-O bond at 40 K. (c) Temperature dependence of $\sigma^2_{M\text{-}O_p}$ for the x=0.05 samples.

ture dependence of in-plane M-O (M=Mn, Ni, and Co) bond MSRD $\sigma^2_{M\text{-}O_p}$ is shown in Fig. 9(c). The upturn of $\sigma^2_{Mn\text{-}O_p}$ below ~100 K is consistent with the existence of the two Mn-O bond distances. The gradual decrease in $\sigma^2_{Ni\text{-}O_p}$ and $\sigma^2_{Co\text{-}O_p}$ with decreasing temperature indicates the absence of local lattice instability around Ni and Co atoms. The Mn, Ni, and Co K-edge EXAFS data constitute direct information on the local lattice structures around these dopants. For the Mn dopants, the beat feature and an upturn of $\sigma^2_{Mn\text{-}O_p}$ appear at low temperature (<100 K), indicating the occurrence of local lattice instability around the Mn dopants. By contrast, no

TABLE I. The average in-plane Cu-O bond distance and the M-O bond distance (M=Mn, Ni, and Co) for the $La_{1.85}Sr_{0.15}Cu_{1-x}M_xO_4$ (M=Mn, Ni, and Co) single-crystal samples taken at 300 K.

Sample composition	In-plane Cu-O bond distance (Å)	In-plane M-O bond distance (Å)
$La_{1.85}Sr_{0.15}CuO_4$	1.885(8)	
Mn doped, x=0.025	1.886(2)	
Mn doped, x=0.03	1.890(1)	
Mn doped, x=0.05	1.892(2)	Mn-O: 1.918(4)
Ni doped, x=0.03	1.886(8)	
Ni doped, x=0.05	1.886(3)	Ni-O: 1.885(6)
Co doped, x=0.05	1.887(4)	Co-O: 1.888(2)

evidence of local lattice instability is observed in Ni- and Co-doped samples. These results suggest that the Mn dopants do not suppress local lattice instability while the Ni and Co dopants strongly suppress the instability.

We also find that the substitution of Mn, Ni and Co at the Cu site leads to a noticeable change in the in-plane Cu-O and M-O (M=Mn, Ni, and Co) bond distances. In Table I we list the typical bond distances for these samples at 300 K. It is found that Mn doping leads to a monotonic increase in the in-plane Cu-O bond distance while the Ni and Co doping changes the Cu-O bond distance only slightly. For the M-O bond distance, the average in-plane Mn-O bond distance is slightly longer than the Cu-O bond distance while the in-plane Ni-O and Co-O bond distances are comparable to the Cu-O bond distance.

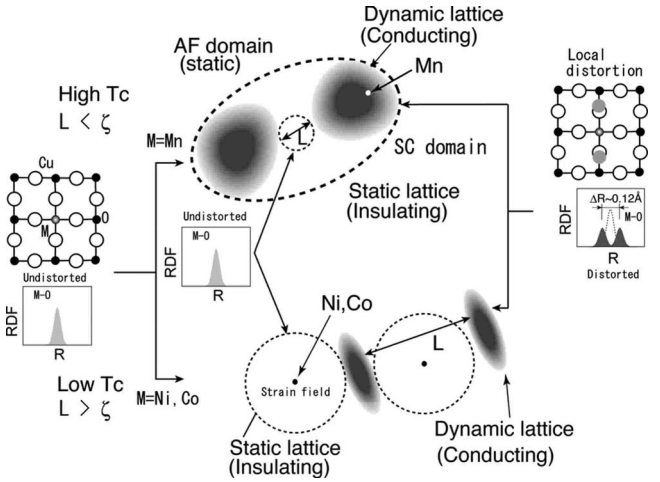

FIG. 10. Schematic of electronic inhomogeneity model illustrating the different perturbations on the local lattice structure induced by Mn, Ni, and Co doping. Dynamic metallic domains (shaded by gray color) are formed as the result of electronic phase separation. Mn dopants do not suppress the dynamic lattice instability. Ni and Co dopants disrupt the dynamic local lattice fluctuation around them and lead to the formation of static distorted domains (circled area) due to the effect of strain field.

D. Lattice instability and superconductivity

We now make some discussion on the local lattice instability and its interplay with superconductivity. A spatial inhomogeneity model is schematized in Fig. 10. Below T^*, local lattice instability occurs which leads to phase separation into metallic domains and insulating ones.[1,25–27] If the distance between adjacent metallic domains (L) is shorter than a critical length ζ, tunneling between the metallic domains is allowed. Phase coherence is achieved when the quantum tunneling threshold is reached. The formation of macroscopic superconducting state is through the spreading of phase coherence by tunneling over the static insulating domains.[28–30] Difference between Mn and Ni (or Co) doping is due to the fact that Mn atoms conserve the local dynamic domains while the Ni and Co dopants make the local lattice distortion "static" because of the strain field. Around the Ni and Co dopants, the static lattice distortion is temperature independent, which is consistent with the term σ_{imp}^2 in Eq. (2). In Ni- and Co-doped samples, dopants lead to the decrease in dynamic regions. The decrease in dynamic regions leads to a decrease in superconducting carrier concentration (n_s), resulting in lower T_c.[31] In this picture, dynamic lattice response plays an important role in HTSC.

IV. CONCLUSION

In conclusion, we present evidence from EXAFS measurements that dynamic local lattice instability occurs in optimally doped $La_{1.85}Sr_{0.15}CuO_4$. The lattice instability occurs only within the CuO_2 plane while it does not involve the apical oxygens. Through the substitution of Mn, Ni, and Co for Cu we find that dynamic lattice instability is intimately related to superconductivity. While Ni and Co suppress the dynamic instability and quench superconductivity, the instability remains dynamic around Mn atoms and the onset superconducting transition temperature keeps nearly constant. These results indicate that the local lattice instability may play an important role in the occurrence of HTSC.

ACKNOWLEDGMENTS

The authors express their thanks to K. A. Müller and A. Bussmann-Holder for their valuable comments and discussions. The EXAFS experiments were conducted under the Proposals No. 2006G117, No. 2006G118, and No. 2007G071 at Photon Factory. This work was partially supported by Japan Society for the Promotion of Science (JSPS).

*Author to whom correspondence should be addressed; h.oyanagi@aist.go.jp

[1] J. Zaanen and O. Gunnarsson, Phys. Rev. B **40**, 7391 (1989).
[2] J. G. Bednorz and K. A. Müller, Z. Phys. B: Condens. Matter **64**, 189 (1986).
[3] V. J. Emery, S. A. Kivelson, and J. M. Tranquada, Proc. Natl. Acad. Sci. U.S.A. **96**, 8814 (1999).
[4] C. C. Homes, S. V. Dordevic, G. D. Gu, Q. Li, T. Valla, and J. M. Tranquada, Phys. Rev. Lett. **96**, 257002 (2006).
[5] N. B. Christensen, H. M. Rønnow, J. Mesot, R. A. Ewings, N. Momono, M. Oda, M. Ido, M. Enderle, D. F. McMorrow, and A. T. Boothroyd, Phys. Rev. Lett. **98**, 197003 (2007).
[6] J. Zaanen, Nature (London) **440**, 1118 (2006).
[7] R. Khasanov, A. Shengelaya, A. Maisuradze, F. La Mattina, A. Bussmann-Holder, H. Keller, and K. A. Müller, Phys. Rev. Lett. **98**, 057007 (2007).
[8] T. Kato, S. Okitsu, and H. Sakata, Phys. Rev. B **72**, 144518 (2005).
[9] K. Terashima, H. Matsui, T. Sato, T. Takahashi, M. Kofu, and K. Hirota, Phys. Rev. Lett. **99**, 017003 (2007).
[10] D. Reznik, L. Pintschovius, M. Ito, S. Iikubo, M. Sato, H. Goka, M. Fujita, K. Yamada, G. D. Gu, and J. M. Tranquada, Nature (London) **440**, 1170 (2006).
[11] C. J. Zhang, H. Oyanagi, and C. H. Lee, Physica C **468**, 898 (2008).
[12] H. Oyanagi, A. Tsukada, M. Naito, N. L. Saini, M.-O. Lampert, D. Gutknecht, P. Dressler, S. Ogawa, K. Kasai, S. Mohamed, and A. Fukano, J. Synchrotron Radiat. **13**, 314 (2006).
[13] J. J. Rehr, J. Mustre de Leon, S. I. Zabinsky, and R. C. Albers, J. Am. Chem. Soc. **113**, 5135 (1991).
[14] A. Bianconi, N. L. Saini, A. Lanzara, M. Missori, T. Rossetti, H. Oyanagi, H. Yamaguchi, K. Oka, and T. Ito, Phys. Rev. Lett. **76**, 3412 (1996).
[15] N. L. Saini, A. Lanzara, H. Oyanagi, H. Yamaguchi, K. Oka, T. Ito, and A. Bianconi, Phys. Rev. B **55**, 12759 (1997).
[16] N. L. Saini, H. Oyanagi, V. Scagnoli, T. Ito, K. Oka, and A. Bianconi, Europhys. Lett. **63**, 125 (2003).
[17] H. Oyanagi, A. Tsukada, M. Naito, and N. L. Saini, Phys. Rev. B **75**, 024511 (2007).
[18] J. Supercond., special issues 1–2, edited by K. A. Müller, D. Mihailovic, and A. Bussmann-Holder, Vol. **17**, pp. 1–324 (2004).
[19] Y. Seino, A. Kotani, and A. Bianconi, J. Phys. Soc. Jpn. **59**, 815 (1990).
[20] G. I. Bersuker and J. B. Goodenough, Physica C **274**, 267 (1997).
[21] A. Bussmann-Holder, A. Simon, and H. Büttner, Phys. Rev. B **39**, 207 (1989).
[22] A. Bussmann-Holder, H. Keller, A. R. Bishop, A. Simon, and K. A. Müller, J. Supercond. Novel Magn. **21**, 353 (2008).
[23] R. P. Sharma, S. B. Ogale, Z. H. Zhang, J. R. Liu, W. K. Chu, Boyed Veal, A. Paulikas, H. Zheng, and T. Venkatesan, Nature (London) **404**, 736 (2000).
[24] G. Dalba and P. Fornasini, J. Synchrotron Radiat. **4**, 243 (1997).
[25] A. Perali, C. Castellani, C. Di Castro, and M. Grilli, Phys. Rev. B **54**, 16216 (1996).
[26] E. Manousakis, Phys. Rev. B **67**, 195103 (2003).
[27] L. P. Gor'kov and G. B. Teitel'baum, J. Phys.: Conf. Ser. **108**, 012009 (2008).
[28] J. Eroles, G. Ortiz, A. V. Balatsky, and A. R. Bishop, Int. J. Mod. Phys. B **15**, 1613 (2001).

[29] A. Bussmann-Holder, K. A. Müller, R. Micnas, H. Büttner, A. Simon, A. R. Bishop, and T. Egami, J. Phys.: Condens. Matter **13**, L169 (2001).
[30] V. V. Kabanov, T. Mertelj, and D. Mihailovic, J. Supercond. Novel Magn. **19**, 67 (2006).
[31] Y. J. Uemura, G. M. Luke, B. J. Sternlieb, J. H. Brewer, J. F. Carolan, W. N. Hardy, R. Kadono, J. R. Kempton, R. F. Kiefl, S. R. Kreitzman, P. Mulhern, T. M. Riseman, D. Ll Williams, B. X. Yang, S. Uchida, H. Takagi, J. Gopalakrishnan, A. W. Sleight, M. A. Subramanian, C. L. Chien, M. Z. Cieplak, Gang Xiao, V. Y. Lee, B. W. Statt, C. E. Stronach, W. J. Kossler, and X. H. Yu, Phys. Rev. Lett. **62**, 2317 (1989).